Magnetic hysteresis from the geometrical barrier in type-II superconducting strips

M. Benkraouda and John R. Clem

Ames Laboratory and Department of Physics and Astronomy, Iowa State University, Ames, Iowa 50011

The magnetic hysteresis due to the geometrical barrier in a type-II superconducting strip placed in a perpendicular applied field is examined theoretically. We first consider ideal strips with no bulk pinning and show results for the average flux density as a function of the applied field for both flux entry and exit. The magnetization is found to be nearly inversely proportional to the applied field upon flux entry and to be proportional to the applied field upon flux exit. We also present results showing the time evolution of magnetic-flux and current-density profiles during initial flux entry for samples that are bulk-pinning free and those with pinning characterized by a critical current J_c. As predicted theoretically in pinning-free strips, the vortices collect in a dome-shaped magnetic flux profile, within which the current density is zero. A vortex-free region develops near the edges, where a high current density flows. With bulk pinning, the vortices pile up in two symmetric dome-shaped magnetic flux profiles, within which the current density is equal to the critical current density, whereas the regions near the center and the edges of the strip remain vortex-free.

I. INTRODUCTION

The first penetration of magnetic flux into a type-II superconducting strip subjected to a perpendicular magnetic field has been found to be significantly delayed by a potential barrier of geometrical origin.[1–3] An important consequence of this effect is that such a strip exhibits strongly hysteretic behavior even if the vortices in the interior of the strip are completely unpinned, i.e., even if the bulk critical current density J_c is zero. This geometrical barrier is due solely to the shape of the sample's cross section at the edge of the strip; it is similar to the barrier observed in type-I superconductors of rectangular cross section,[4] but is different from the Bean-Livingston surface barrier observed in type-II superconductors.[5–9]

The geometrical barrier arises because Meissner screening currents, flowing on the top and bottom surfaces of a flat strip, arise in response to an applied magnetic field.[1–3] The directions of these currents are such that, if one vortex is nucleated at the strip's edge, the resulting Lorentz force on the vortex tends to drive it towards the center of the strip. For a vortex at the very edge of the strip, however, its line tension initially opposes the inward Lorentz force and keeps the vortex near the edge. As the applied field increases until the vortex straightens and spans between the flat surfaces of the strip, the line tension no longer produces a significant outward force, and the vortex is driven to the middle of the sample. This inward motion occurs rapidly and dissipates energy. If the applied field is now reduced, the Lorentz force on the vortex from the Meissner screening currents still keeps the vortex in the middle of the sample until the applied field drops below zero, at which point the Lorentz force reverses sign and drives the vortex out of the sample.

A long sample of elliptical cross section would not exhibit this kind of geometrical barrier, because for this sample shape the inward Lorentz force arising from the Meissner screening currents has exactly the same spatial dependence as that of the outward force arising from line tension.[1–3,10]

Once the field at the edge of the sample reaches the lower critical field H_{c1}, a vortex can be nucleated. A slight further increase of the applied field causes the vortex to move slowly to the middle of the sample. A slight reduction of the applied field, on the other hand, causes the vortex to leave the sample.

The time dependence of flux penetration into a strip with radiation-enhanced edge pinning was studied by Schuster *et al.*,[2] who solved a nonlinear integro-differential equation for the time-dependent current density in the strip. They used a model for the local effective resistivity of the form $\rho = (J/J_c)^n \rho_0$, where $n \gg 1$ and the critical current density $J_c(r, B_z)$ depends upon both the position r and the perpendicular induction B_z. To simulate the behavior in vortex-free regions where $B_z = 0$, the authors formally put $J_c = \infty$ in order to make $\rho = 0$ there.

The steady-state current and field profiles produced in a strip with a geometrical barrier were found analytically by Zeldov *et al.*[3] In their model, vortices were assumed initially to reversibly enter a beveled edge region within a distance $d/2$ of the edge. The diverging Meissner screening currents were cut off at a value of $J_E^0 = 2H_{c1}/d$ in this edge region, such that these currents do work $\phi_0 H_{c1}$ per unit length against the line tension in driving each vortex to a distance $d/2$ from the edge. In this paper we study the dynamics of flux penetration using basic assumptions similar to but slightly different from those of Zeldov *et al.*[3]

To treat the process of vortex nucleation, we consider a model strip (width $2W$) that is flat (with thickness $d \ll W$) over most of its cross section but is rounded at the edges, such that the local radius of curvature at the edges is $d/2$; the penetration depth λ is assumed to be somewhat less than $d/2$. We assume that vortices first begin to enter the sample when the local magnetic field at the sample edge (accounting for demagnetizing effects) exceeds the lower critical field H_{c1}. When this happens, each nucleating vortex gradually moves through the rounded edge region to the flat region,
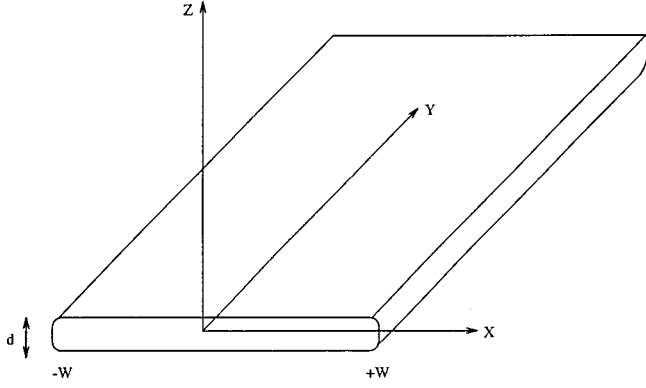
FIG. 1. Sketch of the model superconducting strip considered in this paper. The strip has width $2W$, thickness d, and rounded edges.

where the outwardly directed line-tension force disappears and the inwardly directed screening-current Lorentz force takes over, driving the vortex toward the center of the strip.

To model the flux dynamics, we use Faraday's law to solve for the time dependence of $B_z(x,t)$, the perpendicular component of the flux density in the plane of the strip. In the absence of flux pinning ($J_c=0$), we have $E_y=\rho_{FF} J_y$, where we use the Bardeen-Stephen form[11] of the flux-flow resistivity $\rho_{FF}=\rho_n(B_z/B_{c2})$. This form guarantees that the electric field is zero in any region of the strip that is free of vortices, regardless of the value of the current density J_y. We show, for an applied magnetic field somewhat larger than that required to nucleate the first vortex, how a dome-shaped distribution of $B_z(x,t)$ vs x develops in the middle of a bulk-pinning-free sample. The current density in the vortex-filled region eventually dies away, but the vortex-free region between the sample edges and the vortex-filled dome carries a high current.

This paper is organized as follows: In Sec. II we consider the details of the initial flux penetration into the sample. We then study the quasistatic field (B_z) and current (J_y) distributions that develop at the critical flux-entry and flux-exit conditions, and we calculate for both cases the average flux density and the average magnetization as a function of the applied magnetic field. We find that the magnetization upon flux entry is inversely proportional to the applied field, a behavior that is similar to, but slightly different from, the case of the Bean-Livingston surface barrier.[5–9] In Sec. III we present a straightforward numerical method for calculating the time evolution of $B_z(x,t)$ and $J_y(x,t)$ following flux entry into a type-II superconducting strip. We show that after a long time the profiles of B_z and J_y reduce to those calculated analytically by Zeldov et al.[3] and numerically by Schuster et al.[2] for both bulk-pinning-free samples and those characterized by a critical current density J_c. In Sec. IV we present a brief summary of our results.

II. QUASISTATIC FIELD VARIATIONS

We consider a superconducting strip of width $2W$ and thickness $d \ll W$. To account for demagnetizing effects in calculating the local magnetic field at the edge, we choose a specific model, sketched in Fig. 1, with rounded edges. We now use this model to calculate the Meissner response of the
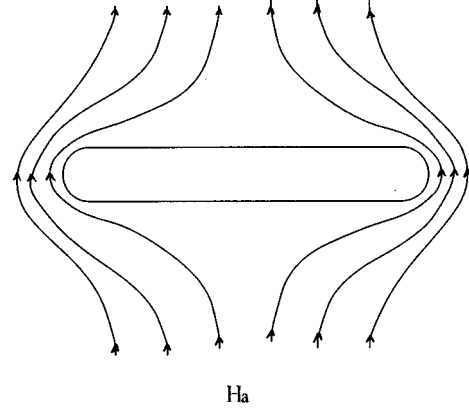
FIG. 2. Sketch of the Meissner-response field around a superconducting strip in the Meissner state in a transverse applied field H_a.

strip, the first vortex penetration into the strip, the vortex-generated current density, the properties at flux entry and flux exit, and the irreversibility line.

A. Meissner response

We first treat the case of a flat strip of thickness d in a uniform magnetic field H_a applied along the z direction (see Fig. 2). The current density is given by

$$J_y = -\left(\frac{\partial H_z}{\partial x} - \frac{\partial H_x}{\partial z}\right). \tag{1}$$

As discussed in Refs. 12–19, it is almost always in strip geometry that the first term on the right-hand side of Eq. (1) can be neglected relative to the second term. Thus Eq. (1) can be rewritten as

$$J_y(x) = \frac{1}{d}[H_x(x,z=d/2)-H_x(x,z=-d/2)]$$

$$= \frac{2}{d}H_x(x,z=d/2), \tag{2}$$

where J_y is the current density averaged over the thickness. Conformal mapping methods can be used to obtain H_{Mx},[20] the Meissner response to the applied field H_a, in the region $|x|<W$,

$$H_{Mx}(x,z=d/2) = -H_a\frac{x}{\sqrt{W^2-x^2}}. \tag{3}$$

The corresponding Meissner-response current density is

$$J_{My}(x) = -\frac{2H_a}{d}\frac{x}{\sqrt{W^2-x^2}}. \tag{4}$$

Equations (3) and (4) hold for all $|x|<W$ except very close to the edge.

To estimate the local magnetic field at the edge of the strip, we consider a model in which the strip's edge is rounded and has radius of curvature $d/2$ at the edge. It is thus useful to examine the Meissner-response field of a long strip with elliptical cross section and compare this with the corresponding Meissner-response field of a flat strip. For a strip

with elliptical cross section, H_{ts}, the tangential field component at the surface of the superconductor, is given by[20]

$$H_{ts} = H_a \frac{L_x + L_z}{2q} \cos\beta, \qquad (5)$$

where $L_x/2$ and $L_z/2$ are the semimajor and semiminor axes of the ellipse, respectively, $q = [(L_x/2)^2 \sin^2\beta + (L_z/2)^2 \cos^2\beta]^{1/2}$, $\cos\beta = x/(L_x/2)$, and the tangent vector is $\mathbf{t} = -\mathbf{x}(L_x/2q)\sin\beta + \mathbf{z}(L_z/2q)\cos\beta$. The parametric equations describing the surface of the ellipse are $x = (L_x/2)\cos\beta$ and $z = (L_z/2)\sin\beta$. The magnitude of the Meissner-response field at either edge $(x = \pm L_x/2)$ is $H_{edge} = H_a(L_x/L_z + 1)$, and the radius of curvature there is $(L_z/2)^2/(L_x/2)$. Choosing L_x to be the strip width $(L_x/2 = W)$ and choosing $d/2$ to be the radius of curvature at the edge $(L_z = \sqrt{2Wd})$, we find that the magnitude of the Meissner-response field at the edge is

$$H_{edge} = H_a(R + 1), \qquad (6)$$

where $R = L_x/L_z = \sqrt{2W/d} \gg 1$. We note that this is the order of magnitude expected from Eq. (3). Evaluating Eq. (3) at $x = -W + d/4$, where we expect the equation to begin breaking down, we get

$$H_{Mx}(x = -W + d/4, z = d/2) \approx H_a R. \qquad (7)$$

Moreover, the z component of the Meissner-response field for a strip of width $2W$ is given outside the strip by[20]

$$H_{Mz}(x, z = 0) = H_a \frac{|x|}{\sqrt{x^2 - W^2}}, \qquad (8)$$

where $|x| > W$. Evaluating this expression at $x = -W - d/4$, where we expect this equation to begin breaking down for a strip of thickness d, we obtain

$$H_{Mz}(-W - d/4, z = 0) \approx H_a R, \qquad (9)$$

in agreement with the estimates from Eqs. (6) and (7).

As pointed out in Ref. 21, it is not a good practice to represent a strip of width $2W$ and thickness d by an inscribed ellipse of semimajor axis W and semiminor axis $d/2$. Such a choice would give a field at the edge [see Eq. (5)] of $H_a(2W/d + 1)$, which is a significant overestimate of the edge field.

Although we do not solve exactly for the tangential field at the surface of the sample sketched in Fig. 1, in the following we use the approximations that the tangential field is given by Eq. (3) on the top surface (and by the negative of this on the bottom surface) when $|x| < W - d/4$ and by Eq. (5) (with $L_x = 2W$ and $L_z = \sqrt{2Wd}$) near the edges of the strip $(W - d/4 < |x| \leq W)$.

B. First vortex penetration into the film

Application of a magnetic field perpendicular to a strip favors the nucleation of vortices at the edges of the strip. The current density induced in response to the applied field produces an inwardly directed force on a nucleating vortex (see Fig. 3). Because of the shape of the strip at its edges, however, each nucleating vortex is also subject to an outwardly
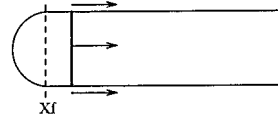
FIG. 3. Sketch showing a vortex near the strip's edge and the inwardly directed force arising from the Meissner-response screening currents.

directed line-tension force. We now examine carefully the balance of forces exerted on a nucleating vortex.

The tangential component (in the direction of $\mathbf{t}$) of the Lorentz force exerted on the top end of a nucleating vortex in a strip of elliptical cross section is, from Eq. (5),

$$F_{ts} = \phi_0 H_{ts} = \phi_0 \frac{H_a(L_x + L_z)}{2q} \cos\beta, \qquad (10)$$

where ϕ_0 is the flux quantum. The work done by the source of the applied field as the vortex moves through a distance Δx into the sample (see Fig. 4) is $\Delta W = 2|F_{ts}|\Delta l$, where $\Delta l = (2q/L_x \sin\beta)\Delta x$ is the distance the top end of the vortex moves along the curving sample surface, and the factor of 2 accounts for the equal amount of work done on the bottom end of the vortex. We thus may write $\Delta W_a = |F_{ax}|\Delta x$, where F_{ax} is the Lorentz force acting in the x direction,

$$F_{ax} = -2\phi_0 \frac{H_a(L_x + L_z)\cos\beta}{L_x \sin\beta}. \qquad (11)$$

When the vortex moves by a distance Δx into the sample, the line energy must increase by $\Delta U = \phi_0 H_{c1}\Delta z$, where H_{c1} is the lower critical field and Δz is the change in the length of the vortex. Since $\Delta z = \Delta x(2L_z/L_x)|\cos\beta|/\sin\beta$, we have $\Delta U = |F_{c1x}|\Delta x$, where the line-tension force acting in the x direction is

$$F_{c1x} = 2\phi_0 \frac{H_{c1}L_z \cos\beta}{L_x \sin\beta}. \qquad (12)$$

When the applied field is small, the Lorentz force F_{ax} is too small to overcome the line-tension force F_{c1x}, and the vortex cannot penetrate into the superconductor. However, from Eqs. (11) and (12), we see that the two forces are balanced when the applied field H_a reaches the value H_p, where
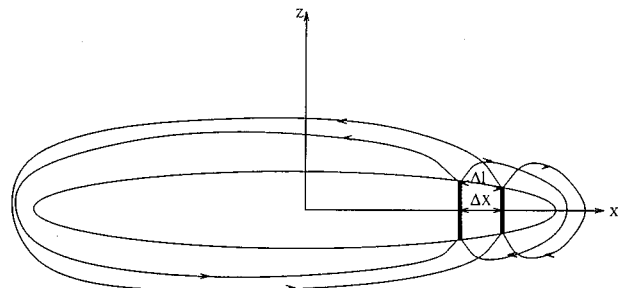
FIG. 4. Sketch of the magnetic field produced outside the sample by a vortex at two positions separated by a distance Δx.

$$H_p = H_{c1} \frac{L_z}{L_x + L_z}. \tag{13}$$

Note that when we chose $L_x = 2W$ and $L_z = \sqrt{2Wd}$, we have

$$H_p = H_{c1} \frac{1}{R+1}, \tag{14}$$

where $R = L_x/L_z = \sqrt{2W/d} \gg 1$. At this field ($H_a = H_p$), the field at the edge of the sample is equal to the lower critical field,

$$H_{\text{edge}} = H_{c1}, \tag{15}$$

as can be seen from Eq. (5). In other words, the vortex will be unable to penetrate the strip until the applied field H_a exceeds H_p, when the Lorentz force from the screening currents overcomes the line-tension force associated with the elliptical shape of the edge. Once the vortex travels a distance $x_f = d/4$ from the edge and the cross section of the strip becomes flat (see Fig. 3), the line tension vanishes and the vortex is now driven rapidly towards the center of the strip where the current density is zero.

For larger values of H_a, this process repeats itself, producing a band of vortices near the center of the strip. The vortices repel each other, and produce a dome-shaped flux distribution within which the total current density is zero. The details of the repulsive vortex interactions are discussed in the next section.

C. Vortex-generated current density

Once the vortices are inside the strip, they generate an upward flux-density contribution $B_z(x)$ in the region $|x| < W$. The magnetic flux density generated by each band of vortices, with flux per unit length $B_z(x')dx'$, returns through the space around the strip, $|x| \gtrsim W$ (see Fig. 4). When $\lambda < d \ll W$, the spatial dependence of this return flux can be calculated by conformal mapping as described in the Appendix of Ref. 10. It follows that the tangential component of the vortex-generated field H_{VTS} on the superconductor's top surface is

$$H_{\text{VTS}} = -\frac{1}{\pi\mu_0 q} \int_{-W}^{+W} dx' \frac{B_z(x')\sqrt{W^2 - x'^2}}{x - x'}, \tag{16}$$

where here, and in what follows, the principal value of the integral is to be taken. Except very near the edges of the strip, we have $q \to W|\sin\beta|$ and $\mathbf{t} \to -\mathbf{x}$ when $d \ll W$, such that the x component of the vortex-generated field on the top surface is

$$H_{vx} = \frac{1}{\pi\mu_0} \int_{-W}^{+W} dx' \frac{B_z(x')\sqrt{W^2 - x'^2}}{(x - x')\sqrt{W^2 - x^2}}. \tag{17}$$

Since the x component of the vortex-generated field on the bottom surface is the negative of this, we find from Eq. (2) that the corresponding vortex-generated current density is (see also Ref. 22)

$$J_{vy}(x) = \frac{2}{\pi\mu_0 d} \int_{-W}^{W} dx' \frac{B_z(x')\sqrt{W^2 - x'^2}}{(x - x')\sqrt{W^2 - x^2}}. \tag{18}$$

The vortices inside the strip thus have two important effects. First, the return flux from the vortex-generated field reduces the field at the edge of the sample. Second, the vortex-generated current density produces a significant contribution to the total current density.

Suppose that a field H_a larger than the value H_p given in Eq. (13) is applied to a sample initially containing no vortices. Since the field at the edge [Eq. (6)] exceeds H_{c1}, vortices nucleate and penetrate into the strip. However, as additional vortices enter the strip and B_z increases, the vortex-generated return flux leads to a negative contribution to H_z at the edge of the strip. The vortex-generated magnetic field $H_{vz}(x = W, z = 0)$ at the edge of the strip is, from Eq. (17),

$$H_{vz}(x = W, z = 0) = -\frac{R}{\pi\mu_0 W} \int_{-W}^{+W} dx' B_z(x') \sqrt{\frac{W+x'}{W-x'}}, \tag{19}$$

where we have made use of $q(\beta = 0) = L_z/2 = \sqrt{Wd/2}$ and $R = \sqrt{2W/d}$. Note that since $B_z(x) > 0$, the vortex-generated field at the edge $H_{vz}(x = W, z = 0)$ is always negative.

The net field at the edge is the sum of the Meissner-response field and the vortex-generated field,

$$H_z(x = W, z = 0) = H_{\text{edge}} + H_{vz}(x = W, z = 0). \tag{20}$$

From Eqs. (6) and (18) we thus obtain

$$H_z(x = W, z = 0) = H_a(R+1)$$
$$-\frac{R}{\pi\mu_0 W} \int_{-W}^{+W} dx' B_z(x') \sqrt{\frac{W+x'}{W-x'}}. \tag{21}$$

As long as $H_z(x = W, z = 0) > H_{c1}$, vortices continue to nucleate and penetrate into the sample, but as more vortices enter the sample, $H_z(x = W, z = 0)$ gradually decreases. Finally, when $H_z(x = W, z = 0)$ drops to the value H_{c1}, vortices will stop entering the sample. We denote the corresponding value of the applied field H_a as the critical entry field H_{en}. If H_a is increased above this value of H_{en}, vortices immediately will begin to enter the sample again.

Just as we can express the net magnetic field as a sum of the Meissner-response field and the vortex-generated field, so also can we express the net current density as the superposition of the Meissner-response current density [Eq. (4)] and the vortex-generated current density [Eq. (18)],[10,20,21,23]

$$J_y(x) = J_{My}(x) + J_{vy}(x). \tag{22}$$

D. Flux entry and flux exit

Let us now vary the applied field H_a quasistatically and find the field and current-density profiles in the cases of both critical flux entry and critical flux exit. The above current-density expressions are sufficient for us to calculate the field profiles inside the sample in the steady state.

1. Flux entry

Consider the condition of critical flux entry, such that the applied field $H_a > H_p$ [Eqs. (13) and (14)], but, because of the return field from the vortices inside the sample, the local field at the sample edge is H_{c1} [Eq. (21)]. Since the sample is
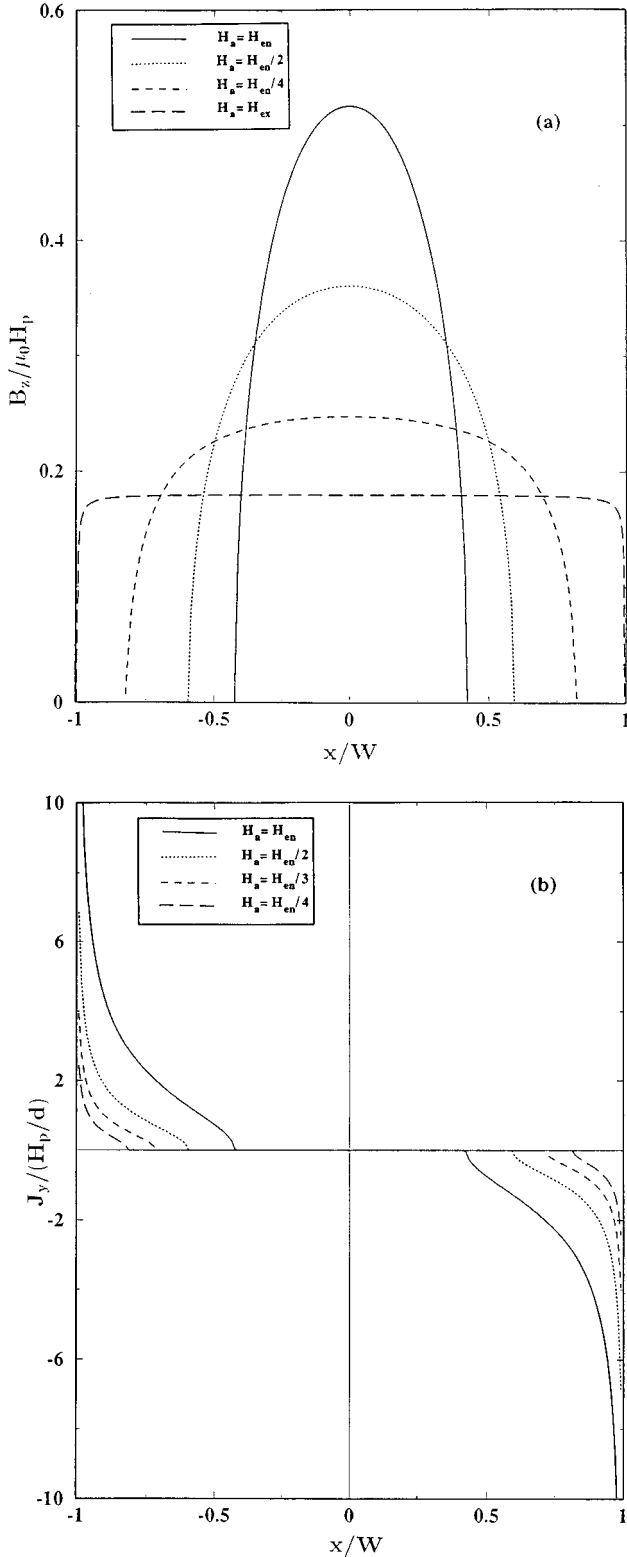
on the verge of nucleating new vortices, we will denote quantities at this critical entry condition by the subscript "en."

We first determine the field profile $B_z(x)$ in the region where vortices have collected. This field profile is symmetric in x, since no transport current is applied, and extends from $-b$ to $+b$, where $0 \leq b < W - d/4$. In order for the vortices to be in equilibrium with each other, each vortex must feel no net Lorentz force; hence the current density $J_y(x)$ must be zero over the region $-b \leq x \leq b$. From Eqs. (22), (4), and (18), we thus obtain

$$J_y(x) = -\frac{2H_a x}{d\sqrt{W^2 - x^2}} + \frac{2}{\pi \mu_0 d}\int_{-b}^{b} dx' \frac{B_z(x')\sqrt{W^2 - x'^2}}{(x - x')\sqrt{W^2 - x^2}}$$

$$= 0. \tag{23}$$

That the solution of this equation is

$$B_z(x) = \mu_0 H_a \sqrt{\frac{b^2 - x^2}{W^2 - x^2}} \tag{24}$$

can be shown with the help of Eq. (7) of Ref. 22.

Outside this region, i.e., $b \leq |x| \leq W$, $B_z(x) = 0$, and the current density, obtained from Eqs. (22), (4), and (18), is

$$J_y(x) = -\frac{2H_a x}{d|x|}\sqrt{\frac{x^2 - b^2}{W^2 - x^2}}. \tag{25}$$

From Eq. (24) we find that the average flux density in the strip is

$$\bar{B}_z = \frac{\mu_0 H_a}{W}\int_0^b dx \sqrt{\frac{b^2 - x^2}{W^2 - x^2}} \tag{26}$$

or

$$\bar{B}_z = \frac{\mu_0 H_a}{W}\frac{b}{W}E(b/W, W/b), \tag{27}$$

where $E(b/W, W/b)$ is an elliptic integral of the second kind.

Because of the symmetry of the current-density distribution, we can write the magnetization as

$$M_z = \frac{1}{W}\int_0^W dx\, x J_y(x). \tag{28}$$

Using Eq. (25) and carrying out the integral, we obtain

$$M_z \approx -\frac{\pi}{4}H_a R^2(1 - b^2/W^2), \tag{29}$$

where $R = \sqrt{2W/d}$. Corrections to Eq. (29) are required, however, when b becomes close to W. In this case, more careful attention must be paid to the contribution of currents that flow on the rounded edges of the sample.

The above expressions [Eqs. (24)–(29)] hold for arbitrary values of H_a and b. However, as H_a is increasing, the value of b at the critical entry condition, i.e., b_{en}, is determined from Eq. (21) by setting the right-hand side equal to H_{c1}, using Eq. (24), and carrying out the required integral. The expression from which $b_{en}(H_a)$ can be obtained is

FIG. 5. (a) Flux-density profiles B_z vs x for an applied field H_a initially at H_{en} and then at smaller fields $H_{en}/2, H_{en}/4$, and H_{ex}, the critical exit field, for $R = 10.05$ and $H_{en} = 1.2H_p$. (b) Current-density profiles J_y vs x for an applied field H_a initially at H_{en} and then at smaller fields $H_{en}/2, H_{en}/3$, and $H_{en}/4$, for $R = 10.05$ and $H_{en} = 1.2H_p$.

$$H_a = \frac{H_{c1}}{1 + R\sqrt{1 - (b_{en}/W)^2}}. \tag{30}$$

The average flux density $\bar{B}_{en}(H_a)$ in the strip at the critical entry condition is, from Eq. (27),

$$\bar{B}_{en} = \frac{\mu_0 H_a}{W} \frac{b_{en}}{W} E(b_{en}/W, W/b_{en}). \tag{31}$$

The magnetization $M_{en}(H_a)$ for increasing field H_a is, from Eq. (29),

$$M_{en} = \begin{cases} -\dfrac{\pi}{4} H_a R^2 & \text{for } H_a < H_p, \\[2mm] -\dfrac{\pi}{4} (H_{c1} - H_a)^2 / H_a & \text{for } H_a > H_p. \end{cases} \tag{32}$$

When $R \gg 1$, we see from Eqs. (14) and (32) that when $H_a \sim H_p \ll H_{c1}$, we have $M_{en} \approx -\frac{\pi}{4} H_{c1}^2 / H_a$, a result close to that found in Ref. 3. This feature appears to be characteristic of the geometrical barrier.

The above procedure determines $b_{en}(H_a)$ and $\bar{B}_{en}(H_a)$ as functions of an increasing field H_a. Alternatively, one may also regard b_{en} and the critical entry field H_{en} (the value of H_a at the critical entry condition) as functions of the average flux density $\bar{B}$. One may combine Eqs. (30) and (31) to eliminate H_a in favor of b_{en}; one may then determine $b_{en}(\bar{B})$ from the resulting equation. In turn, $H_{en}(\bar{B})$ can be determined by using $b_{en}(\bar{B})$ in Eq. (30).

2. Flux exit

Suppose that we have increased the applied field H_a to some maximum value H_{en} above H_p. Since additional vortices have just entered into the strip, the width of the vortex-filled strip, $2b_{en}$, and the average flux density in the strip, $\bar{B}_{en}$, can be determined from Eqs. (30) and (31) by replacing H_a by H_{en}.

When we now reduce the applied field H_a, the total number of vortices in the strip remains constant (and thus the average flux density $\bar{B}_z$ remains constant), but the value of b increases. We can use Eqs. (27) and (31) to derive an equation for determining b under decreasing H_a, as long as $\bar{B}$ is constant:

$$H_a \frac{b}{W} E(b/W, W/b) = H_{en} \frac{b_{en}}{W} E(b_{en}/W, W/b_{en}). \tag{33}$$

By substituting the resulting value of $b(H_a)$ into Eq. (29), we can determine the corresponding magnetization M_z at this value of H_a.

No vortices will exit the strip until the outermost vortices at $|x| = b$ reach the rounded edge of the strip at $|x| = b_{ex} \equiv W - d/4$. When this occurs, since the field
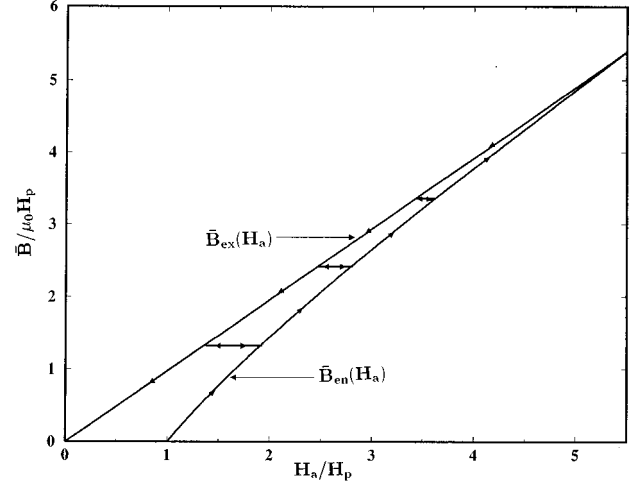
FIG. 6. The average flux density $\bar{B}$ as a function of the applied field H_a at the critical entry condition ($\bar{B}_{en}$, increasing fields), the critical exit condition ($\bar{B}_{ex}$, decreasing fields), and the constant-flux condition ($H_{ex} < H_a < H_{en}$) for $R = 10.05$.

$H_z(|x| = W, z = 0) < H_{c1}$, the outermost vortices will exit the sample. We denote the value of H_a at which flux exit occurs for this value of $\bar{B}$ as $H_{ex}(\bar{B})$. It is determined via Eq. (33) from

$$H_{ex} \frac{b_{ex}}{W} E(b_{ex}/W, W/b_{ex}) = H_{en} \frac{b_{en}}{W} E(b_{en}/W, W/b_{en}), \tag{34}$$

where $b_{ex} = W - d/4$.

For decreasing applied fields H_a at the critical exit condition, we thus have $b_{ex} = W - d/4$ (independent of H_a), while the average flux density in the sample, $\bar{B}_{ex}(H_a)$, is determined via Eq. (27) from

$$\bar{B}_{ex} = \frac{\mu_0 H_a}{W} \frac{b_{ex}}{W} E(b_{ex}/W, W/b_{ex}), \tag{35}$$

and the magnetization $M_{ex}(H_a)$ is given via Eq. (29) by

$$M_{ex} \approx -\frac{\pi}{4} H_a \tag{36}$$

when $R \gg 1$.

Shown in Fig. 5(a) is a plot of several profiles of $B_z(x)$ vs x as the applied field H_a is reduced from its initial value H_{en} to the corresponding critical exit field H_{ex}. The area under each curve, which is proportional to the average flux density $\bar{B}$, is constant. Note also that b increases as H_a decreases. Several plots of the current density $J_y(x)$ vs x are shown in Fig. 5(b). Since the magnitude of $J_y(x)$ decreases as H_a decreases, the magnitude of the magnetization also decreases.

The average flux density $\bar{B}$ is shown in Fig. 6 as a function of the applied field H_a. For increasing fields at the critical entry condition, $\bar{B} = \bar{B}_{en}$ [Eq. (31)], while for decreasing fields at the critical exit condition, $\bar{B} = \bar{B}_{ex}$ [Eq. (35)].

Note that $\bar{B}$ is constant for $H_{ex} < H_a < H_{en}$, because the geometrical barrier prevents vortices from entering or leaving the sample.

Shown in Fig. 7 is b, the half-width of the vortex-filled region, as a function of H_a. For increasing fields at the critical entry condition, $b = b_{en}$, which is determined from Eq. (30), and for decreasing fields at the critical exit condition, $b = b_{ex} = W - d/4$. As H_a is varied from H_{en} to H_{ex} the expansion of the vortex-filled region is given by Eq. (33). The arrows pointing in both directions on these curves indicate that, in the absence of bulk pinning, this breathing motion of the vortex-filled region is reversible.

Figure 8 shows the magnetization M_z as a function of the applied field H_a. The magnetization for increasing H_a is given by Eq. (32), first for $H_a < H_p$ in the Meissner state and then for $H_a > H_p$ at the critical entry condition. The magnetization for decreasing H_a at the critical exit condition is given by Eq. (36). The magnetization on the reversible branches between these limiting curves corresponds to the reversible breathing motion of the vortex-filled region, and the values of M_z are calculated from Eq. (29) using values of b obtained from Eq. (33).

E. Irreversibility line

From Figs. 6–8 and the corresponding equations we see that the curves of $\bar{B}_{en}$ and $\bar{B}_{ex}$ converge, as do the curves of b_{en} and b_{ex} and those of M_{en} and M_{ex}, at an applied field given by Eq. (30) when $b_{en} = b_{ex} = W - d/4$, or $H_{irr} \approx H_{c1}/2$. For $H_a < H_{irr}$, the magnetization is hysteretic (irreversible), but for $H_a > H_{irr}$, the hysteresis arising from the geometrical barrier completely disappears, though it is possible that hysteresis from a Bean-Livingston barrier or bulk pinning (neither of which has been considered here) may still be present. Note that the temperature dependence of the irreversibility field H_{irr} is the same as that of H_{c1}.

Vortices are generally not present in the rounded edges of the strip when $H_a < H_{irr}$. They appear there only briefly as they move inward at the critical entry condition or outward at the critical exit condition. For $H_a > H_{irr}$, however, vortices are forced into the rounded-edge region. In equilibrium, no net currents flow in the flat region of the film; otherwise, the vortices would move under the influence of the Lorentz force. Thus the entire magnetization of the strip arises from the surface currents in the rounded-edge region. The local surface-current density is proportional to the discontinuity in the tangential component of $\mathbf{B}$ at the film edges.

Exactly at $H_a = H_{irr}$, the value of B in the rounded-edge region is zero and the net field at the edge is H_{c1}. The current carried by the rounded edge at $x = W$ is approximately $I_y(x=W) \approx -H_{c1}d$. From an expression similar to Eq. (28) we thus find that the magnetization is $M_z \approx -H_{c1}$.

For applied fields larger than H_{irr}, the net field at the edge, H_{edge}, rises above H_{c1}, and the value of the flux density just inside the rounded-edge region is determined by the equilibrium curve $B_{eq}(H_{edge})$. Although it is not possible with the present model to accurately calculate H_{edge}, we can show, using Eq. (21), that this field approaches the applied
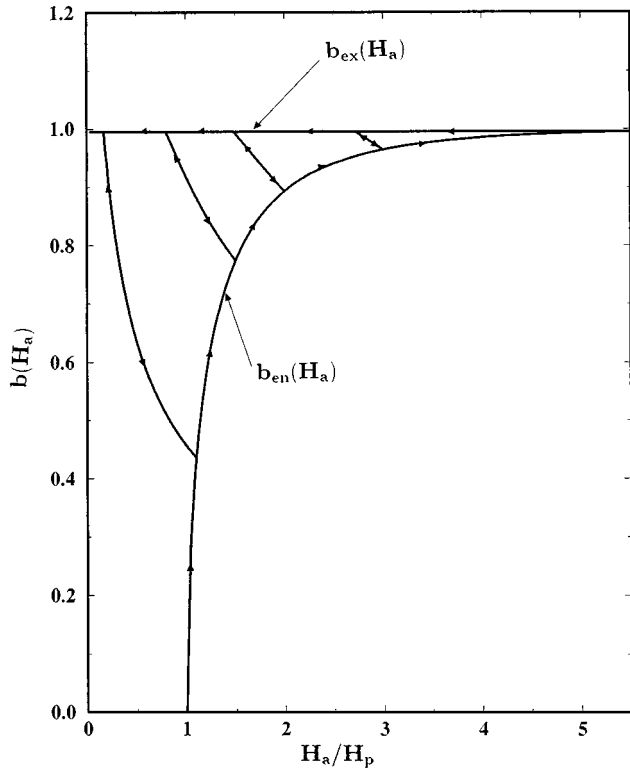
FIG. 7. The behavior of b, the edge of the vortex-filled region, as a function of the applied field H_a at the critical entry condition (b_{en}, increasing fields), the critical exit condition (b_{ex}, decreasing fields), and the constant-flux condition ($H_{ex} < H_a < H_{en}$) for $R = 10.05$.
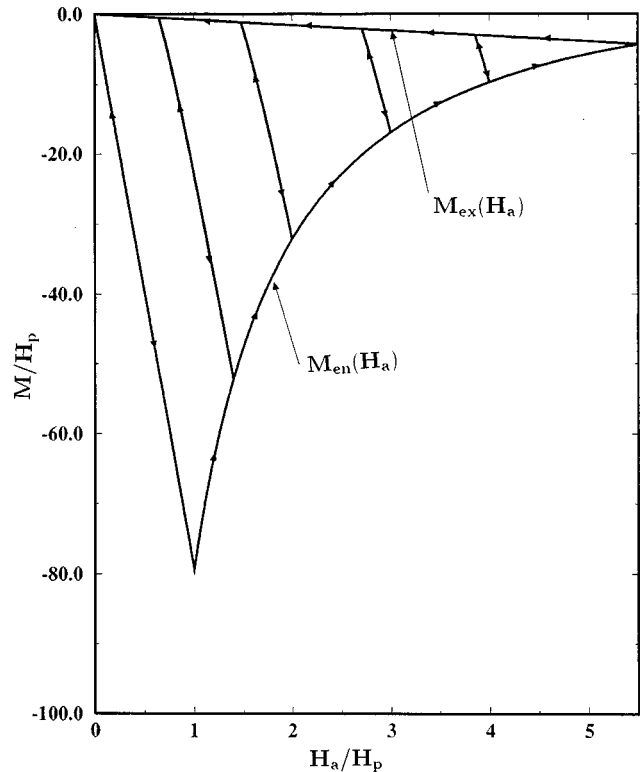
FIG. 8. The magnetization M_z as a function of the applied field H_a at the critical entry condition (M_{en}, increasing fields), the critical exit condition (M_{ex}, decreasing fields), and the constant-flux condition ($H_{ex} < H_a < H_{en}$) for $R = 10.05$.

field H_a. The sample magnetization M_z, arising from the surface-current density in the rounded-edge region, therefore approaches the equilibrium (reversible) magnetization $M_{eq}(H)$. Note that in the mixed state, $M_{eq}(H_{c1}) = -H_{c1}$, and that it decreases in magnitude with increasing field H.

III. TIME EVOLUTION OF THE FLUX PENETRATION

A. Pinning-free samples

We now examine how the flux penetration occurs with time and how the dome-shaped field profile is reached, taking into account the geometrical barrier. Since our calculations are done numerically, we can even include the other part of the current [see Eq. (1)], which is due to the gradient of the thermodynamic field, $-\partial H_z/\partial x$. In the case of flux flow, we assume that the resistivity is given by the Bardeen-Stephen model[11]

$$\rho_{FF} = \rho_n \frac{B_z}{B_{c2}}, \qquad (37)$$

where ρ_n is the normal resistivity and B_{c2} is the upper critical field. An electric field is produced by the motion of vortices under the influence of the currents in the strip. For flux flow the electric field thus obeys

$$E_y(x) = \rho_{FF} J_y(x), \qquad (38)$$

where J_y [see Eqs. (4) and (18)] is given by

$$J_y(x) = J_{My}(x) + J_{vy}(x) - \frac{\partial H_z(x)}{\partial x}. \qquad (39)$$

Notice that if there are no vortices inside the strip (i.e., if $B_z = 0$), there cannot be any electric field, since ρ_{FF} is proportional to B_z. Faraday's law yields a time-dependent equation for the flux density B_z,

$$\frac{\partial B_z(x,t)}{\partial t} = -\frac{\partial E_y(x,t)}{\partial x}. \qquad (40)$$

Using the previous equations, we obtain an integro-differential equation, which in dimensionless units becomes

$$\frac{\partial b_z(x,t)}{\partial t} = -\frac{\partial}{\partial x}\left[-\frac{h_a b_z(x,t)x}{\sqrt{1-x^2}} + \frac{b_z(x,t)}{\pi} \right.$$
$$\times \int_{-1}^{1} dx' \frac{b_z(x',t)\sqrt{1-x'^2}}{(x-x')\sqrt{1-x^2}}$$
$$\left. -\frac{d}{2}b_z(x,t)\frac{\partial h_z(x,t)}{\partial x} \right], \qquad (41)$$

where x and d are in units of W, $b_z(B_z)$ is in units of $\mu_0 H_{c1}$, $h_a(H_a)$ and $h_z(H_z)$ are in units of H_{c1}, and t is in units of $\tau = B_{c2}Wd/2\rho_n H_{c1}$. For example, for $B_{c2} = 100$ T, $W = 50$ μm, $d = 1$ μm, and $B_{c1} = 10$ mT, we obtain $\tau = 3$ ns.

Equation (41) is solved numerically, taking into account the continuity of H_z at the edges; i.e., at every step of the time integration the field B_z at the edges is adjusted such that
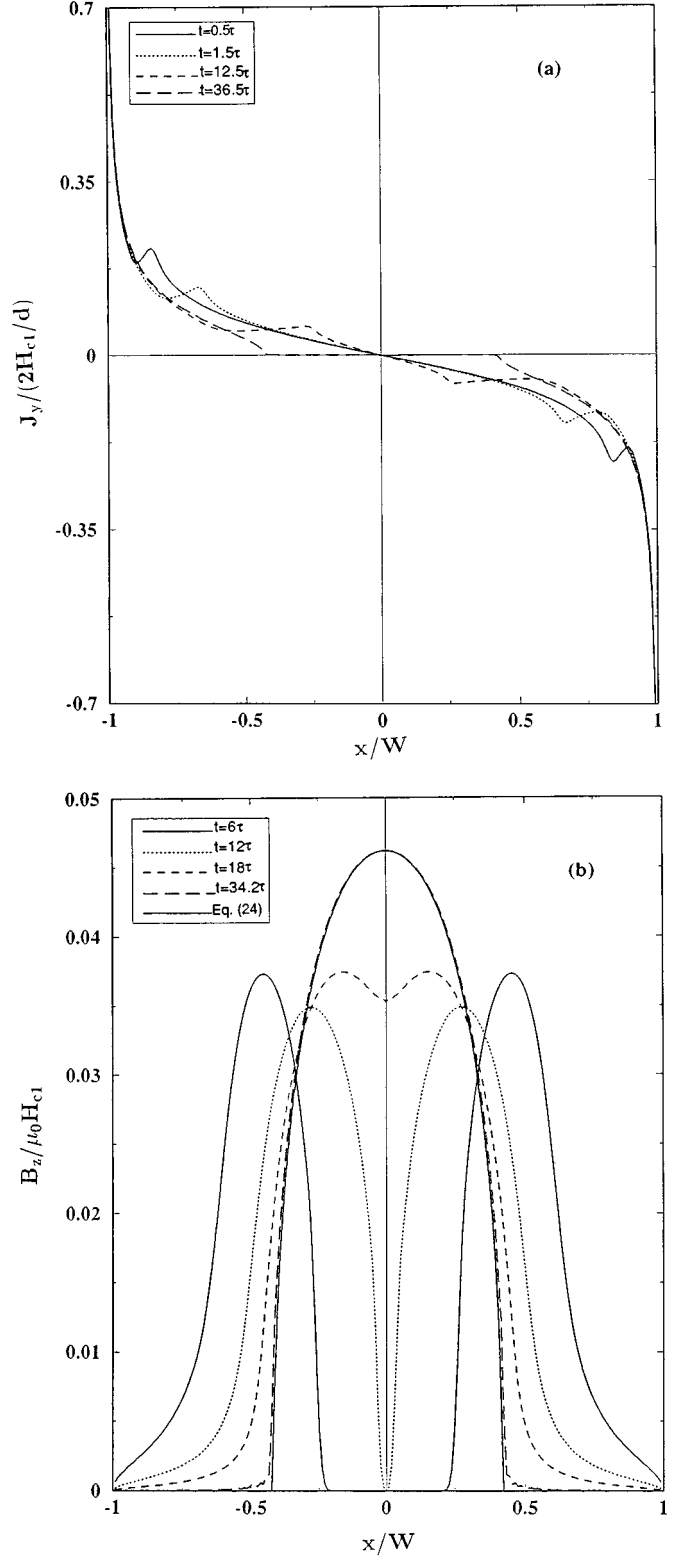
FIG. 9. (a) Current-density profiles for different times t (in units of the characteristic time τ) after an applied field $H_a = 1.2H_p$ is turned on. The numerical results for times greater than $t = 37\tau$ are indistinguishable from the analytical result given in Eq. (25). (b) Field profiles for different times t after an applied field $H_a = 1.2H_p$ is turned on. The numerical results for times greater than $t = 37\tau$ are indistinguishable from the analytical result given in Eq. (24). ($R = 10.05$.)

H_z is continuous there. H_z and B_z are assumed to be related by the equilibrium condition $H = H_{eq}(B)$, which is approximated by the equation[7]

$$H_z(B_z) = \frac{B_z}{|B_z|}\sqrt{H_{c1}^2 + B_z^2/\mu_0^2}.$$ (42)

The exact form of this function is not very important close to the steady state in the range of applied fields, $H_a < H_{irr}$, because in this range the flux density in the steady state is zero at the edges of the strip. When H_z at the strip's edge is equal to or less than H_{c1}, $B_z = 0$ at the edge, and no flux can enter the strip.

When an applied field $H_a > H_p$ is suddenly applied to a strip containing no vortices, the field H_z at the edge is initially greater than H_{c1}, and vortices are admitted into the sample. The net field H_z at the edge is the sum of two contributions, one due to the applied field and the other due to the return flux that arises from vortices that have penetrated into the strip. The return flux produced by the vortices entering the sample gradually reduces the value of H_z at the edge down to H_{c1}. At this point, no additional vortices can penetrate the strip. The vortices inside the sample, however, keep moving toward the center of the strip under the influence of the current density $J_y(x,t)$, in such a way that the current density becomes zero in the vortex-filled region when the vortices achieve their final distribution [see Figs. 9(a) and 9(b)]. The steady-state profiles of both the field and the current density are very nearly the same as those obtained in Sec. II, where we neglected the current part due to the gradient of H_z,

$$B_z(x) = \begin{cases} H_a \sqrt{\dfrac{b^2 - x^2}{W^2 - x^2}} & \text{for } |x| < b, \\ 0 & \text{for } b < |x| < W, \end{cases}$$

$$J_y(x) = \begin{cases} 0 & \text{for } |x| < b, \\ -\dfrac{x}{|x|}\dfrac{2H_a}{d}\sqrt{\dfrac{x^2 - b^2}{W^2 - x^2}} & \text{for } b < |x| < W, \end{cases}$$ (43)

and b is given by Eq. (30).

The main difference between our numerical results and the profiles shown in Ref. 3 is in the details of how the edges are treated. In Ref. 3, the current density is cut off there at J_E^0. In addition, the slope of B_z at $\pm b$ in our treatment is no longer infinite because we have included the term $-\partial H_z/\partial x$ in the expression of the current J_y. The dome-shaped magnetic flux profile has been seen experimentally by both Zeldov *et al.*[3] and Schuster *et al.*[2]

B. Samples with bulk pinning

In the presence of bulk pinning characterized by a critical current density J_c, we model the electric field as in Ref. 24,

$$E_y(x,t) = \begin{cases} \rho_{FF}[J_y(x,t) - J_c] & \text{for } J_y(x,t) > J_c, \\ 0 & \text{for } |J_y(x,t)| < J_c, \\ \rho_{FF}[J_y(x,t) + J_c] & \text{for } J_y(x,t) < -J_c. \end{cases}$$ (44)

Different field and current profiles are obtained, depending on the values of H_a and J_c. The most interesting case is when $H_a > H_p$, such that vortices penetrate into the sample, but J_c is smaller than J_y at the edges. As shown in Figs. 10(a) and 10(b), vortices enter the strip until the field at the edge is reduced to H_{c1}, and under the influence of the current J_y the vortices are pushed towards the center. Because of
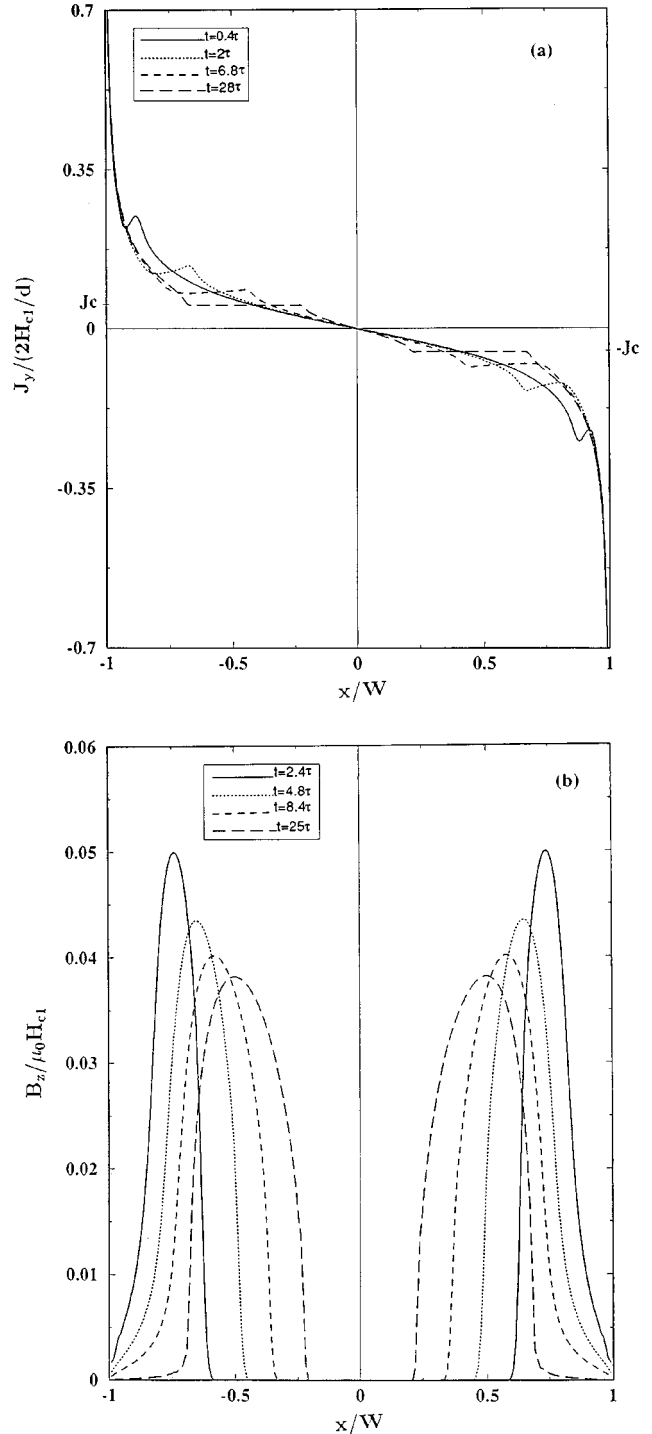
FIG. 10. (a) Current-density profiles for different times t (in units of the characteristic time τ) after an applied field $H_a = 1.2 H_p$ is turned on, for the case of bulk pinning characterized by a critical current density $J_c = 1.1 H_p/d$. (b) Field profiles for the same conditions as in (a).

the E-J relationship given above, however, the vortices come to rest when $|J_y| \lesssim J_c$. The vortices therefore pile up in two symmetric regions where the current is reduced to J_c. The rest of the sample is vortex free, and the current density greatly exceeds J_c at the edges [see Figs. 10(a) and 10(b)]. The final field and current-density profiles are similar to those obtained by Zeldov *et al.*[3] except for details of the behavior at the edges. In the case of large J_c, the steady-state profiles approach the analytical results obtained in Refs. 21, 23.

IV. SUMMARY

In this paper we have studied the effects of the geometrical barrier that impedes vortex entry and exit in type-II superconducting strips. We have used a specific model, a strip that is mostly flat but has rounded edges, to estimate the magnetic fields and currents in the strip. The key contributions are (a) the Meissner response to a transverse applied field and (b) fields and currents generated by vortices in the strip. By considering the effects of demagnetization, we determined H_p, the value of the applied field at which the local magnetic field at the edge of the strip first reaches the lower critical field H_{c1}. For increasing fields $H_a > H_p$, when vortices are present in a dome-shaped field distribution in the strip, we calculated the flux-density and current-density distributions at the critical entry condition. If the applied field is subsequently reduced, the geometrical barrier prevents vortices from immediately leaving the sample. No vortices leave the sample until the outermost vortices reach the rounded edge of the strip, the critical exit condition. We calculated hysteresis in the magnetization M_z, including M_{en} at the critical entry condition for increasing H_a, M_{ex} at the critical exit condition for decreasing H_a, and the reversible magnetization in the constant-flux condition for applied fields between H_{ex} and H_{en}.

We also investigated vortex dynamics in strip geometry by numerically solving a time-dependent equation governing the penetration of B_z into the strip. We presented plots of B_z and J_y showing the time evolution of these distributions after a transverse magnetic field is applied. We showed that these distributions closely approach those calculated analytically.

Although most of this paper concerned the behavior of vortices in a strip in which there is no bulk or surface pinning, we also briefly considered the vortex dynamics in a strip with bulk pinning to show how the flux distributions are altered. In confirmation of results reported in Ref. 3, we find that the vortices penetrate from both edges and collect in two dome-shaped distributions, within which the magnitude of the current density is J_c.

Note that our results for $J_c = 0$ exhibit hysteresis (irreversibility) in the magnetization even though pinning plays no role whatsoever. The hysteresis arises entirely from the effects of sample geometry, as noted in Refs. 1–3. We calculated an irreversibility field H_{irr}, the value of the applied field ($\sim H_{c1}$), above which the magnetization becomes completely reversible.

A possible extension of the present approach would be to relax the condition of continuity of H_z at the edge of the sample, which would permit the study of the Bean-Livingston barrier in strip geometry. It is likely that this would increase not only the value of the applied field at which the first vortex penetration would occur but also the value of the irreversibility field H_{irr}.

Further studies of vortex dynamics, including numerical studies of ac losses at arbitrary frequencies, would also be possible using Eq. (41). Vortex distributions during flux flow under the influence of a transport current also could be easily computed using our approach.

[1] M. V. Indenbom, H. Kronmüller, T. W. Li, P. H. Kes, and A. A. Menovsky, Physica C **222**, 203 (1994).

[2] Th. Schuster, M. V. Indenbom, H. Kuhn, E. H. Brandt, and M. Konczykowski, Phys. Rev. Lett. **73**, 1424 (1994).

[3] E. Zeldov, A. I. Larkin, V. B. Geshkenbein, M. Konczykowski, D. Majer, B. Khaykovich, V. M. Vinokur, and H. Shtrikman, Phys. Rev. Lett. **73**, 1428 (1994).

[4] J. Provost, E. Paumier, and A. Fortini, J. Phys. F **4**, 439 (1974).

[5] C. P. Bean and J. D. Livingston, Phys. Rev. Lett. **12**, 14 (1973).

[6] John R. Clem, in *Proceedings of the Conference on Low Temperature Physics*, edited by K. D. Timmerhaus, W. J. O'Sullivan, and E. F. Hammel (Plenum, New York, 1974), Vol. 3, p. 102.

[7] J. R. Clem, J. Appl. Phys. **50**, 3518 (1979).

[8] L. Burlachkov, Phys. Rev. B **47**, 8056 (1993).

[9] A. Buzdin and D. Feinberg, Phys. Lett. A **165**, 281 (1992).

[10] J. R. Clem, R. P. Huebener, and D. E. Gallus, J. Low Temp. Phys. **6**, 449 (1973).

[11] J. Bardeen and M. J. Stephen, Phys. Rev. **140**, A1197 (1965).

[12] H. Theuss, A. Forkl, and H. Kronmüller, Physica C **190**, 345 (1992).

[13] D. J. Frankel, J. Appl. Phys. **50**, 5402 (1979).

[14] M. Däumling and D. C. Larbalestier, Phys. Rev. B **40**, 9350 (1989).

[15] L. W. Conner and A. P. Malozemoff, Phys. Rev. B **43**, 402 (1991).

[16] L. W. Conner, A. P. Malozemoff, and I. A. Campbell, Phys. Rev. B **44**, 403 (1991).

[17] J. R. Clem, in *Proceedings of the 7th International Workshop on Critical Currents in Superconductors*, Alpbach, Austria, 1994, edited by Harald W. Weber (World Scientific, Singapore, 1994), p. 117.

[18] E. H. Brandt, Phys. Rev. Lett. **71**, 2821 (1993).

[19] E. H. Brandt, Phys. Rev. B **49**, 9024 (1994).

[20] R. P. Huebener, R. T. Kampwirth, and J. R. Clem, J. Low Temp. Phys. **6**, 275 (1972).

[21] E. Zeldov, J. R. Clem, M. McElfresh, and M. Darwin, Phys. Rev. B **49**, 9802 (1994).

[22] E. H. Brandt, Phys. Rev. B **46**, 8628 (1992).

[23] E. H. Brandt, M. V. Indenbom, and A. Forkl, Europhys. Lett. **22**, 735 (1993).

[24] Y. B. Kim and M. J. Stephen, in *Superconductivity*, edited by R. D. Parks (Marcel Dekker, New York, 1969), Vol. 2, Chap. 19, p. 1107.